JOURNAL OF SOLID STATE CHEMISTRY 90, 126–146 (1991)

Electrical Switching of Two-Phase ZnO–$PrCoO_3$ Threshold Switching Materials

KWANGSOO NO* AND MICHAEL F. BERARD

The Engineering Research Institute and the Department of Materials Science and Engineering, Iowa State University, Ames, Iowa 50011

Received March 21, 1988; in revised form August 3, 1990

Electrical switching of ZnO–Pr_6O_{11}–Co_3O_4 ceramics was investigated. The roles of individual grains and interphase boundaries in the electrical switching behavior of bulk two-phase threshold switching material based on ZnO–Pr_6O_{11}–Co_3O_4 were studied using microelectrodes deposited photolithographically on a thin section of the material. The materials consists of Co-doped ZnO and Zn-doped $PrCoO_3$ phases. Pristine Co-doped ZnO grains showed high "off" state resistance and a high threshold switching voltage for the initial voltage sweep and were permanently conductive for subsequent sweeps. "Damage traces" were observed in these grains after initial switching. Zn-doped $PrCoO_3$ grains exhibited stable and reproducible threshold switching behavior. Through the study of the electrical characteristics of single-phase polycrystalline undoped and Co-doped ZnO materials and undoped and Zn-doped $PrCoO_3$ materials, the microelectrode observations of the switching behavior of the two-phase material were confirmed. Undoped ZnO showed n-type semiconductivity with a resistivity of around 1 Ω-cm. Doping ZnO with Co increased this resistivity. Evidence was obtained that the resistivity increase in ZnO accompanying doping with Co was not due to blocking contacts. Undoped and Zn-doped $PrCoO_3$ showed p-type semiconductivity with a resistivity of around 100 Ω-cm. Doping $PrCoO_3$ with Zn decreased the resistivity. A blocking contact was observed between $PrCoO_3$ and electrode metals having low work function. A microstructural model of the switching behavior of two-phase ZnO–$PrCoO_3$ material is proposed on the basis of this study.

Introduction

Certain zinc oxide ceramics exhibit current-controlled negative resistance (CCNDR) behavior (*1*) or memory switching behavior (*2, 3*). Recently, Hunter and Schaefer (*4*) found that ZnO-based ceramics can be made to exhibit CCNDR, memory switching, and/or threshold switching behaviors depending on the particular additive oxide compositions. They identified the best compositions for threshold switching materials, which consisted of combinations of ZnO, Pr_6O_{11}, and Co_3O_4. However, the sintered tablets of these compositions disintegrated into powder after standing in laboratory air for several days to several months, depending on the composition and fabrication technique. The objectives of this study were (1) to stabilize the microstructure of the materials so as to avoid disintegration and (2) to study the electrical characteristics of the individual phases in the two-phase microstructure and single phase polycrystalline materials having similar composition to the individual phases in order to arrive at a bet-

* Present address: Department of Materials Science and Engineering, Korea, Advanced Institute of Science and Technology, Taejon, Korea.

0022-4596/91 $3.00

ter understanding of the bulk switching behavior of these ceramics.

Experimental Procedure

Specimen Preparation

Three different types of materials were chosen for study: two-phase threshold switching materials, single-phase polycrystalline undoped and Co-doped ZnO materials, and single-phase polycrystalline undoped and Zn-doped $PrCoO_3$ materials. The starting materials used to fabricate the two-phase threshold switching ceramics were ZnO, Pr_6O_{11}, and Co_3O_4. It is known that praseodymium oxide disproportionates into PrO_2 and $Pr(OH)_3$ on long exposure to laboratory air (*5*). Therefore, the concentration of Pr in the praseodymium oxide was determined using atomic absorption spectroscopy after decomposition of residual $Pr(OH)_3$ by calcining in air at 800°C for 2 hr. This calcined powder of known Pr content was weighed out for mixing with the other oxides in all batches. Before being mixed with ZnO, the praseodymium oxide and Co_3O_4 materials were prereacted to $PrCoO_3$. This was accomplished by mixing the two powders for 4 hr in a plastic vial with plastic balls using a SPEX mill, and then heating in air in an alumina crucible at 1200°C for 40 hr. Repeated grinding and heating were used to convert the entire batch to $PrCoO_3$. After grinding, the $PrCoO_3$ powder (30 wt%) was mixed with ZnO using a SPEX mill. The as-received ZnO powder was of very fine particle size, which would result in a relatively fine-grained sintered microstructure. For certain two-phase specimens in which microelectrode arrays were to be deposited, it was necessary to prepare large particle size ZnO using a technique known as the seed grain method (*6*). These particular two-phase switching ceramics are called "large grain threshold switching materials."

Two different cobalt oxide powders were blended for 4 hr with ZnO to prepare single-phase polycrystalline Co-doped ZnO materials for fabrication and sintering. Mixing was performed in a plastic vial with plastic balls using a vibration mill. The mean particle size of the as-received Co_3O_4 powder was 14.5 μm. It was suspected that this particle size was so much larger than that of the ZnO powder (1.1 μm) that it would be difficult to produce a uniform distribution of Co throughout the ZnO. Consequently, a portion of the as-received Co_3O_4 powder was jet milled to a mean particle size of 4.4 μm before being blended with the ZnO powder. A second group of specimens was prepared with CoO powder (3.8 μm mean particle size) to determine whether the oxidation state of Co in the starting powder had an effect on the electrical characteristics of the Co-doped ZnO produced. Efforts to fabricate Zn-doped $PrCoO_3$ specimens by repeatedly heating and grinding a mixture of ZnO, Co_3O_4, and Pr_6O_{11} powders were unsuccessful. The microstructure of the reacted materials did not show a homogeneous Zn-doped $PrCoO_3$ phase, but rather two phases were always observed in the microstructure. Therefore, two-phase materials which consisted of Co-doped ZnO and Zn-doped $PrCoO_3$ phases were first produced, and the Co-doped ZnO phase was then leached out using a 10 *M* NaOH solution at 100°C to leave behind grains of Zn-doped $PrCoO_3$. Specimens were fabricated from this leached powder. After powder mixtures were prepared, the mixtures were pressed in a 1.27-cm diameter steel die to form cylinderical tablets having a thickness between 0.3 and 1 cm, and then were isostatically pressed at 30,000 psi. The tablets were sintered in air at 1300°C for 10 hr. After sintering, the tablets were sliced to obtain cylindrical specimens with varous thicknesses. The faces of these specimens were ground flat on a 600 mesh SiC grinding disk and were polished with 0.3 μm alumina powder.

In–Ga metal electrodes were painted onto both surfaces of the bulk specimens. To study the electrical characteristics of individual grains and interphase boundaries in two-phase threshold switching materials, an array of aluminum microelectrodes was deposited onto the one polished surface using photolithographic and sputtering techniques after the specimens had been thinned to several tens of microns thickness. During thinning, the section was observed through a transmission optical microscope to confirm that the final specimen thickness encompassed only one grain for ZnO grains. For $PrCoO_3$ grains, this observation could not be made, because this phase is not transparent at these specimen thicknesses.

Measurements

Direct current-voltage characteristics were measured using a curve tracer as a power supply. The current-voltage data were obtained using digital multimeters and were acquired and manipulated using a microcomputer and peripherals interfaced using a general purpose interface bus (GPIB). The samples were tested on Cu block (heat sink), and the time interval between consecutive sweeps was always at least 1 day. The dc resistivities of some specimens were also measured using a four-point probe method (*7*). The type of majority carriers in the materials was determined using a hot probe technique (*8*). The grain and interfacial (electrode and intergranular) contributions to total specimen resistance were separated by ac complex impedance spectroscopy (*9*).

To study the electrical characteristics of individual grains and interphase boundaries in two-phase threshold switching materials, an array of microelectrodes was fabricated onto the surface of the thin section of the materials. When, by chance, electrode pairs were located on interesting grains or on either side of grain and interphase boundaries, two ultrasharp measurement probes were located on the pair using a micromanipulator. Traces of the dc current-voltage characteristics between these microelectrodes were made on the screen of a storage curve tracer.

The microstructures of the switching ceramics being studied were observed using an optical microscope and a scanning electron microscope with energy dispersive X-ray spectroscopy capability. Thin sections of undoped and Co-doped ZnO grains are transparent to visible light so that the doping profile in this material could be observed on the basis of the transmitted color difference between undoped ZnO (pale yellow) and Co-doped ZnO (green). The doping profile within a grain was also observed using energy dispersive X-ray spectroscopy. Powder X-ray diffraction patterns were produced using a diffractometer to determine phase(s) present in the materials. The chemical compositions of the materials were determined using atomic absorption spectroscopy. The particle size distribution of powders was analyzed using a sedimentation method.

Results and Discussion

Microstructural Stabilization

The threshold switching materials identified by Hunter and Schaefer (*4*) were fabricated using mixtures of ZnO, Pr_6O_{11}, and Co_3O_4 powders. After sintering, the tablets generally had low porosity and good mechanical strength. However, the sintered tablets disintegrated into powder after standing in laboratory air for from several days to several months, depending on composition and fabrication technique. As the Pr and Co oxide content increased, the tablets disintegrated faster. When the powder mixture was calcined before the tablets were formed, the disintegration was delayed, but the tablets eventually turned to powder after a long period of time. It is known that Pr_6O_{11} disproportionates into PrO_2 and $Pr(OH)_3$ with long exposure to laboratory air. During

the disproportionation, the volume of the original praseodymuin oxide phase will be changed. The associated internal stresses would be expected to crack sintered tablets if they contain unreacted Pr_6O_{11}. However, pure Pr_6O_{11} tablets were observed in this study to be stable for over a year, so the presence of another Pr-rich oxide phase may be responsible for this problem. The X-ray pattern of the sintered material matched well with the published patterns of ZnO and $PrCoO_3$ (*10*); however, there were several unidentified peaks of low intensity. It was observed in the present study that the interior of the tablet always started to distintegrate first. This observation suggests that the problem was not due to disproportionation, because the reaction requires moisture and would be expected to start at the surface of the tablet.

Whatever the cause of tablet disintegration, a solution was suggested by the X-ray diffraction pattern, which showed that the threshold switching material consists of two major phases: ZnO and $PrCoO_3$. Since a praseodymium oxide phase is not needed for switching and seems to be responsible for tablet disintegration, this phase was eliminated by prereacting Pr_6O_{11} and Co_3O_4 to prepare $PrCoO_3$ powder prior to its being added to ZnO powder. It was found that the $PrCoO_3$ powder used for mixing with ZnO required some excess Co, because some Co will diffuse into the ZnO grains during sintering, resulting in residual unreacted praseodymuim oxide being present in the materials, causing the tablets to eventually disintegrate into powder. Tablets fabricated using prereacted Co-excess $PrCoO_3$ powder have been found to be stable in air for at least several years.

Microstructure

Figure 1 shows the microstructure of a two-phase threshold switching material. The material consists of a dispersion of two-major phases. Figure 1b shows traces of the relative intensities of X-rays generated by the electron beam at points along the line indicated in Fig. 1c. The trace of Zn X-ray intensities indicates that Zn is located mainly in the grey phase with minor amounts in the white phase. The trace of Co X-ray intensities shows that Co is present in both the white phase and the grey phase; however, Co content in the white phase is higher than in the grey phase. The trace of Pr X-ray intensities shows that Pr is located only in the white phase. The X-ray diffraction pattern of the material was matched exactly to the published patterns of ZnO and $PrCoO_3$ phases. The combination of X-ray diffraction and elemental analyses identifies the grey phase as ZnO doped with Co that has diffused in from the surrounding $PrCoO_3$ grains, and the white phase as $PrCoO_3$ doped with Zn that has diffused in from the adjacent ZnO grains.

Direct Current-Voltage Characteristics

Figure 2 shows a typical log–log plot of the bulk dc current-voltage characteristics of a two-phase threshold switching ceramic. At low voltage, the material exhibited high resistance ohmic behavior. Above a certain electric field, $E_{NONOHMIC}$, the material changed to nonohmic behavior. The nonlinear exponent was around 4. When the electric field was above a threshold value, E_{TH}, the material switched to the highly conductive "on" state. A load resistor was used to protect the material against an overpower situation after the transition. The current through the material after the transition depended on the magnitude of the load resistor. In the on state, the material exhibited negative differential resistance behavior with a nonlinear exponent around -2 within the current range capable of being tested in this study. Then, as current was reduced, the on state was maintained until the current through the material fell to a holding value, below which the material returned to its

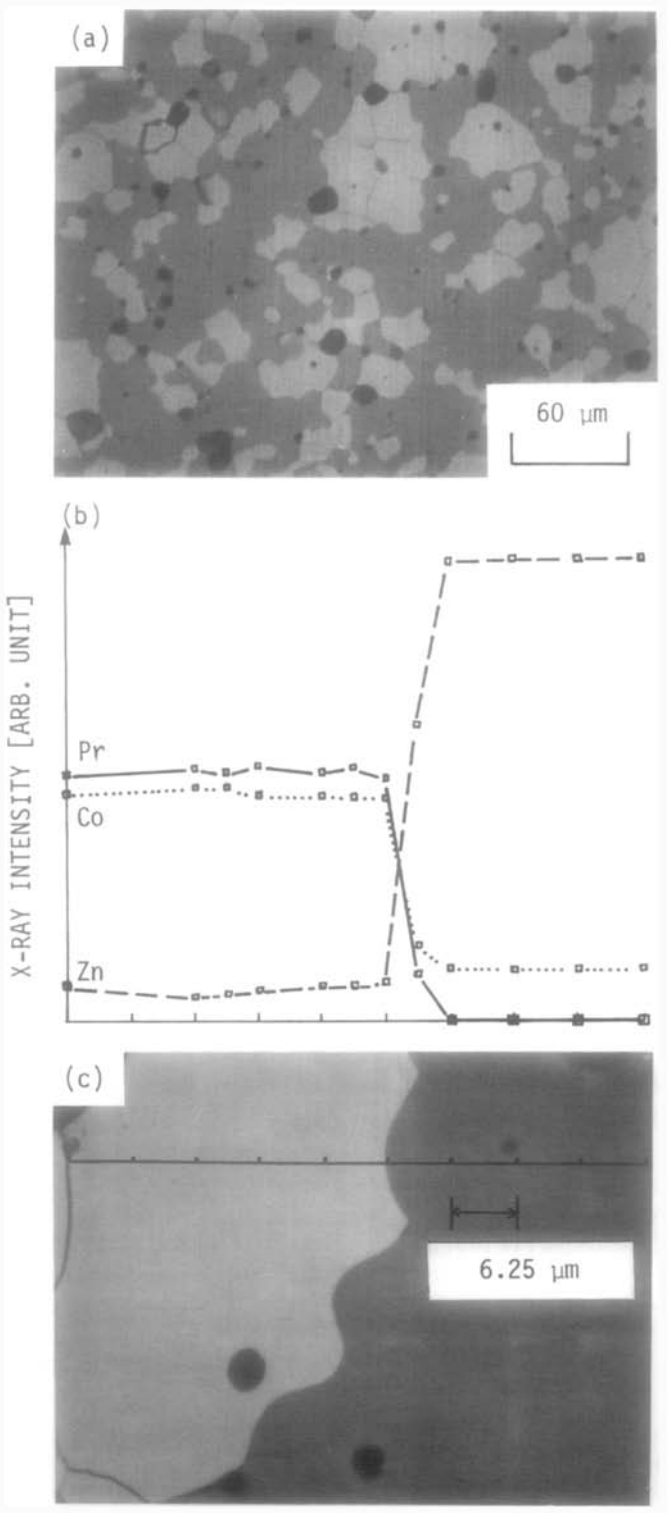

FIG. 1. Microstructure of a two-phase ZnO–$PrCoO_3$ threshold switching material. (a) SEM BSE image, (b) X-ray spectra generated from points along the line in (c).

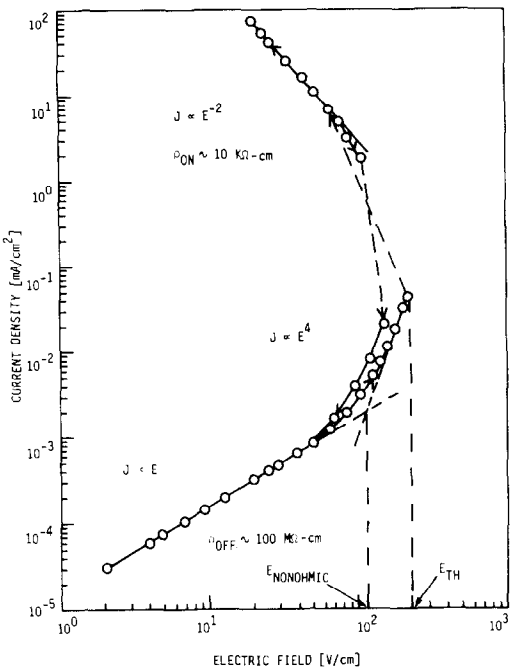

FIG. 2. Direct current-voltage characteristics of a two-phase threshold switching material.

original high resistance off state. The threshold voltage for subsequent sweeps was lower than that for the first sweep (about 50% lower for the second sweep in this sample). All threshold switching materials tested in this study showed a lowering of threshold voltage after the first sweep, with the amount of reduction depending on the current level of the on state for the preceding sweep.

Direct Current-Voltage Characteristics of Individual Grains and Interphase Boundaries

The roles of individual grains and interphase boundaries in the bulk electrical behavior of two-phase threshold switching materials were studied using microelectrode pairs sputtered onto the surface of thinned specimens. The kinds of microstructural features tested between pairs of microelectrodes were (a) a group of several undoped ZnO grains in a polycrystalline pure ZnO specimen; (b) individual Co-doped ZnO grains; (c) groups or clusters of Zn-doped $PrCoO_3$ grains in large grain size threshold switching materials; and (d) a combination of several Co-doped ZnO and Zn-doped $PrCoO_3$ grains in normal two-phase threshold switching materials.

Tests of undoped ZnO grains. An electrode array deposited on a thin section of sintered undoped polycrystalline ZnO is shown in Fig. 3. In this case, it is obvious that each electrode covers a number of grains and grain boundaries. A linear low resistance (around 200 Ω) dc current-voltage trace was observed for groups of several undoped ZnO grains; a typical trace is shown in Fig. 3. Pure ZnO exhibits n-type semiconductivity due to its intrinsic defects (*11*).

Tests of individual Co-doped ZnO grains. Tests with pairs of electrodes on the same Co-doped ZnO grain in large grain size threshold switching material showed a high resistance off state, followed by switching to the on state at a high threshold voltage (around 700 V in this case) on the first sweep, as is shown in Fig. 4. When the current was decreased, the grain did not return to its original high resistance off state, but rather showed unstable conduction all the way back to zero voltage. For subsequent sweeps, e.g., Fig. 4b, the grain did not show any switching, but behaved like the on state of the first sweep, showing unstable conduction.

Careful microstructural examination showed a "damage trace" due to a "breakdown" through the Co-doped ZnO grain after the initial sweep, as is shown in Fig. 4d. The word breakdown is used because the transition to a low resistance on state was not reversible, i.e., the specimen never returned to the high resistance off state. It is important to realize that the difference between switching followed by breakdown and reversible switching is probably just a

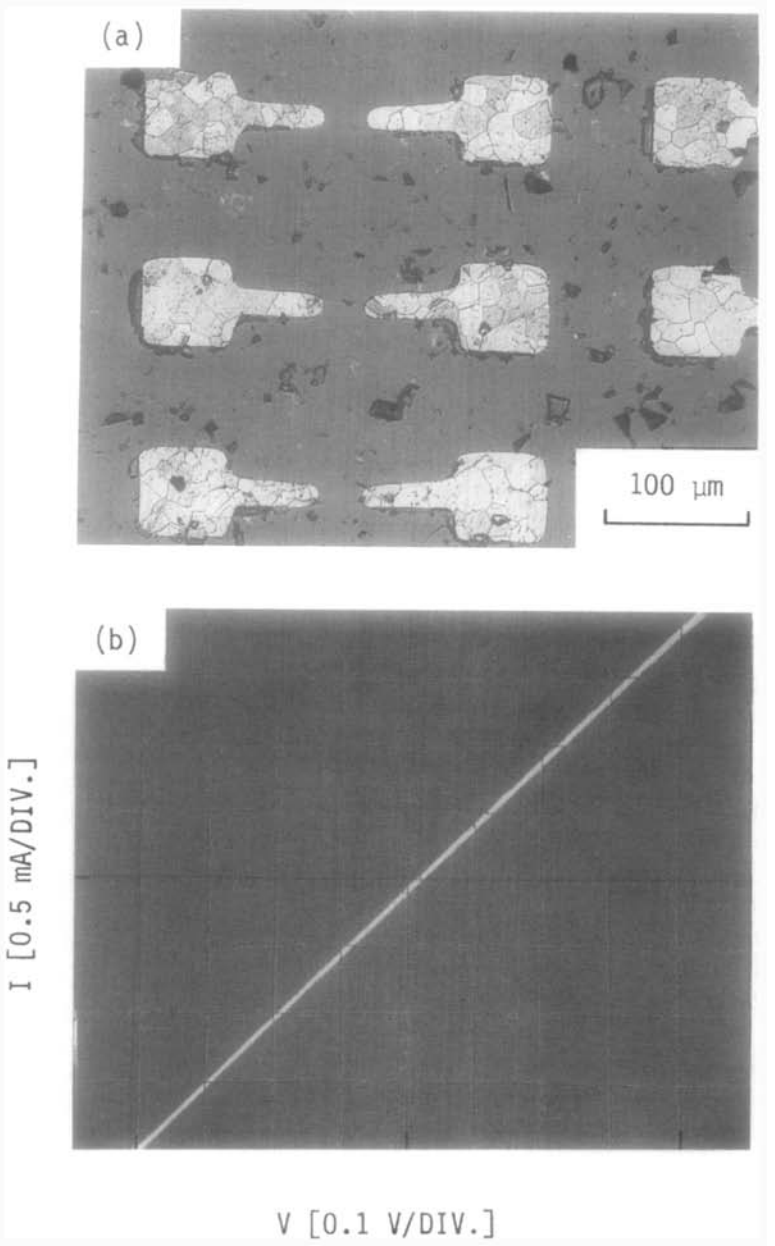

FIG. 3. (a) Microelectrode array deposited on undoped ZnO thin section, (b) a dc current-voltage trace for several undoped ZnO grains.

matter of the magnitude of the current flow permitted in the on state. Figure 4c shows a trace of Co X-ray intensities generated by the electron beam at points along the line indicated in Fig. 4d. Since Co entered the ZnO grain by diffusing in from adjacent $PrCoO_3$ grains, the Co distribution across this ZnO grain was not uniform, being more concentrated in the outer position than in the interior. The ZnO grain appeared to have

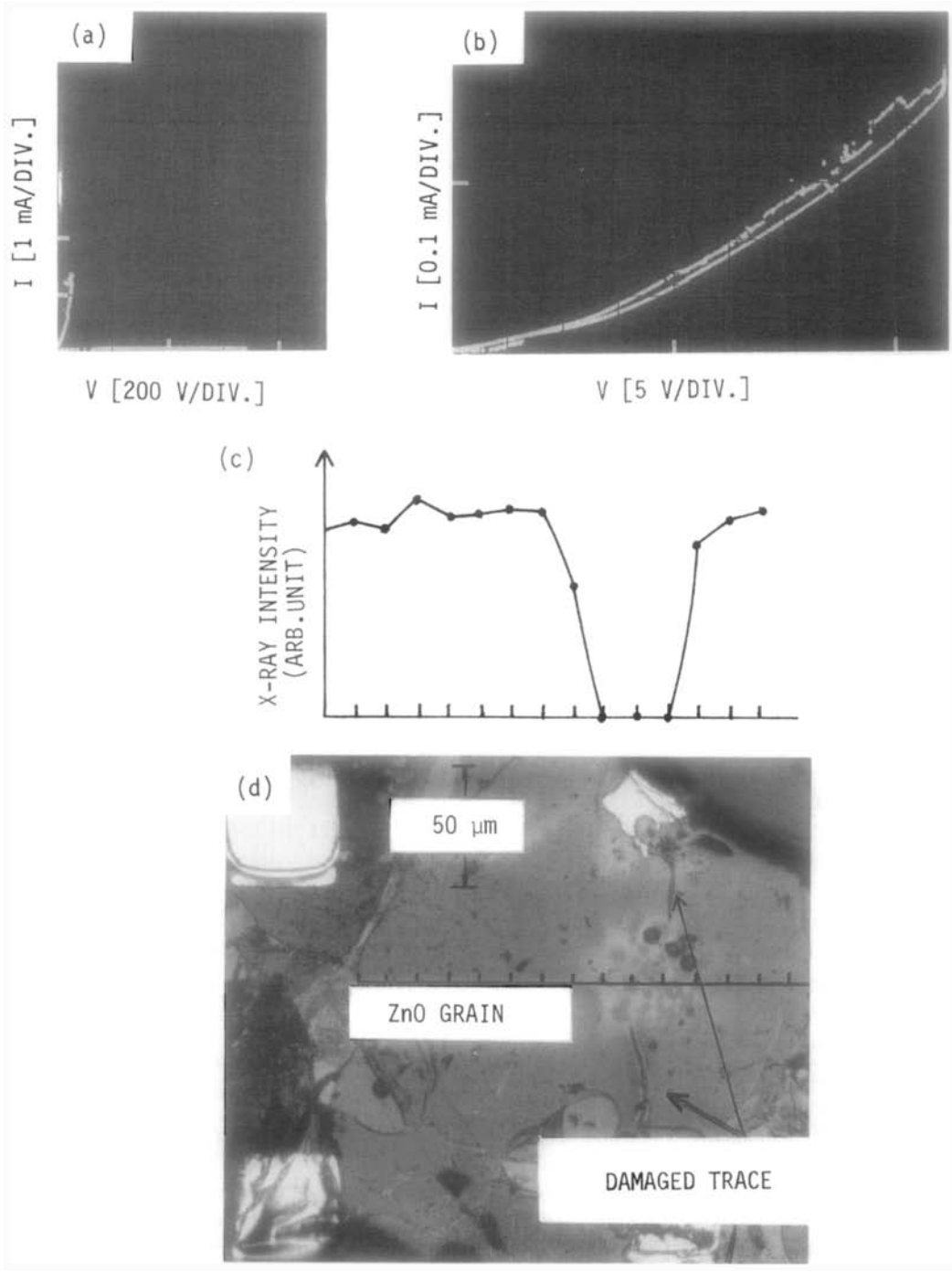

FIG. 4. Direct current-voltage traces for the same single Co-doped ZnO grain for (a) the first sweep and (b) second sweep. (c) Co X-ray spectrum generated from points along the line in (d) the microstructure near a Co-doped ZnO grain after the first sweep.

an undoped region in the center as judged by color in transmitted light. The electrodes were so located as to include both Co-doped and undoped portions of the grain between them. The damage trace is observed only in the outer Co-doped region of the ZnO grain, but not the central undoped region. These observations are consistent with the initial high resistance of the Co-doped ZnO grain being due to a highly resistive Co-doped region, which undergoes breakdown during the first sweep to produce a damage trace which then remains permanently conductive. No such breakdown is needed for conduction to take place through the normally semiconducting undoped region of the ZnO grain. Scanning electron microscopic examination showed that the damage trace was actually a crack. The square in the upper left of Fig. 4d shows a pristine microelectrode as deposited on the thin section. Both of the electrodes used for testing were "burned" during the initial sweep due to high current density following breakdown.

Test of clusters of Zn-doped $PrCoO_3$ grains. Individual Zn-doped $PrCoO_3$ grains were too small to be tested singly using pairs of microelectrodes. Consequently, only the electrical characteristics of clusters of these grains were tested. Clusters of Zn-doped $PrCoO_3$ grains showed stable and reproducible threshold switching, as is shown in Fig. 5. The threshold voltage of the first sweep was much lower than those observed for the first sweep threshold or breakdown voltage of Co-doped ZnO grains. The threshold voltage of subsequent sweeps (above 70 V) in Zn-doped $PrCoO_3$ grains was similar to that of the first sweep (about 110 V). Figure 5c shows the microstructure in the vicinity of the grains tested. A damage trace was not observed in the cluster of grains between the microelectrode pair. Because of high current through the material in the on state, blocking electrodes are easily damaged; in Fig. 5c, the burned electrode was the anode, which is consistent with $PrCoO_3$ exhibiting p-type conductivity (5). A barrier between the metal electrode and a p-type semiconductor blocks hole movement, so that the hole-injecting electrode, the anode, contributes most of the impedance, while the electron-jumping electrode, the cathode, contributes little impedance.

Tests of combinations of Co-doped ZnO and Zn-doped $PrCoO_3$ grains. These combination test paths showed high first sweep threshold voltage (Fig. 6a) and reproducible threshold switching with a lowered threshold voltage for subsequent sweeps (Fig. 6b). The threshold voltages of these combination test paths for subsequent sweeps were similar in magnitude to those observed for clusters of Zn-doped $PrCoO_3$ grains, as discussed above. The combination test path observations are well matched to the dc current-voltage characteristics observed for bulk two-phase threshold switching materials, which always exhibit a higher threshold voltage for the first sweep but a lower threshold voltage for subsequent sweeps. Figure 6c shows that damage traces were observed primarily in Co-doped ZnO grains along the combination test paths. The damage traces did not follow straight line paths between the electrodes, but usually branched into two or three paths. Therefore, the effective area of the current path through the specimen in the on state is probably much smaller than the geometric area of the specimen and is indeterminant.

Electrical Characteristics of Single-Phase Polycrystalline Materials

To further understand the observed switching behavior in two-phase materials, the electrical characteristics were studied for single-phase polycrystalline Co-doped ZnO and Zn-doped $PrCoO_3$, which constitute the individual phases of two-phase threshold switching materials.

Undoped and Co-doped ZnO materials. Figure 7 shows the dc characteristics of single-phase polycrystalline undoped and Co-

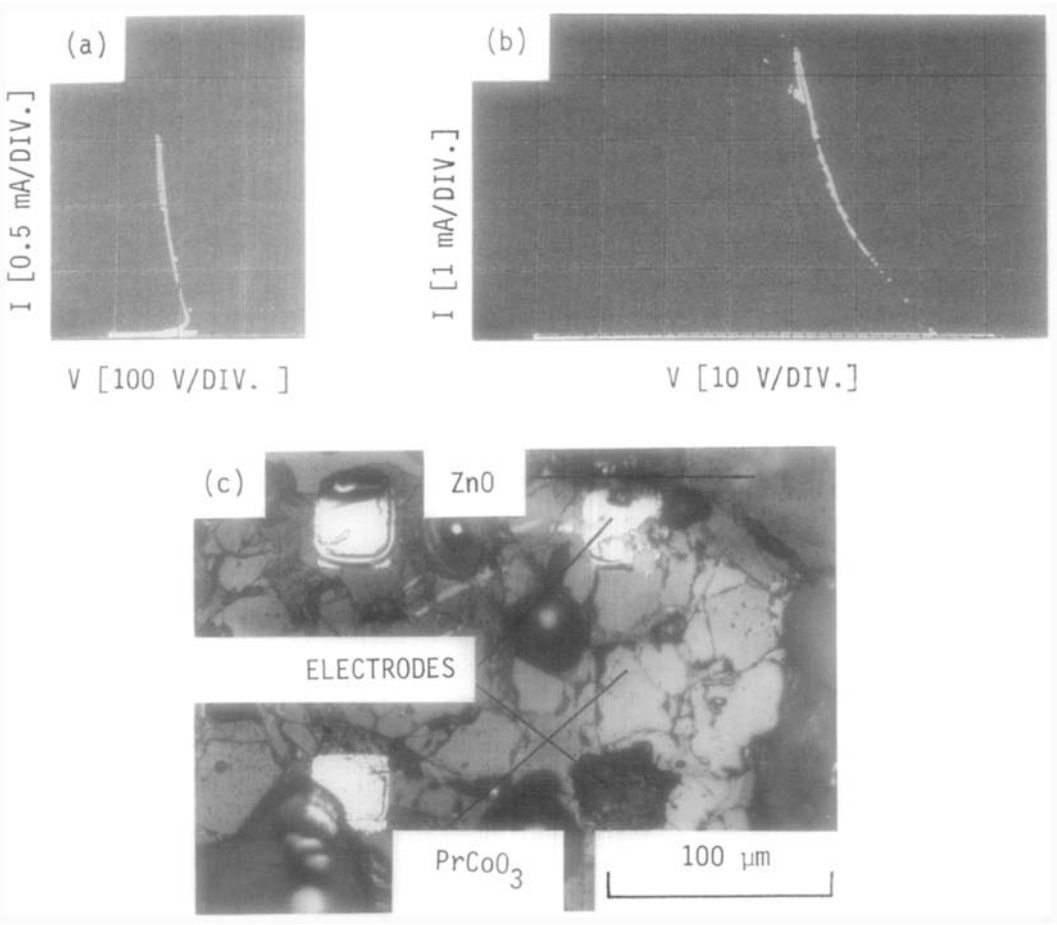

FIG. 5. Direct current-voltage traces for clusters of Zn-doped $PrCoO_3$ grains (a) for the first sweep and (b) after several consecutive sweeps. (c) Microstructure near the cluster of grains tested.

doped ZnO materials prepared with Co_3O_4 powder. Undoped and lightly doped ZnO materials exhibited ohmic behavior over the entire current density range tested in this study. As Co content increased, the materials showed the onset of nonohmic behavior at successively lower current density. The materials having higher doping concentrations exhibited threshold switching behavior. It was expected that these materials would show switching on the initial sweep followed by a permanent conductive state for subsequent sweeps, as had been observed in dc current-voltage characteristics of individual Co-doped ZnO grains in two-phase $ZnO–PrCoO_3$ threshold switching material. However, the heavily Co-doped ZnO single-phase samples tested in this study showed threshold switching (with a lowered threshold voltage) even for subsequent sweeps. It is believed that the difference between switching followed by breakdown (as was observed in the earlier study on individual grains) and the reversible switching (observed here for bulk specimens) is a matter of the magnitude of the current density permitted in the on state. In the present study, the current densities in

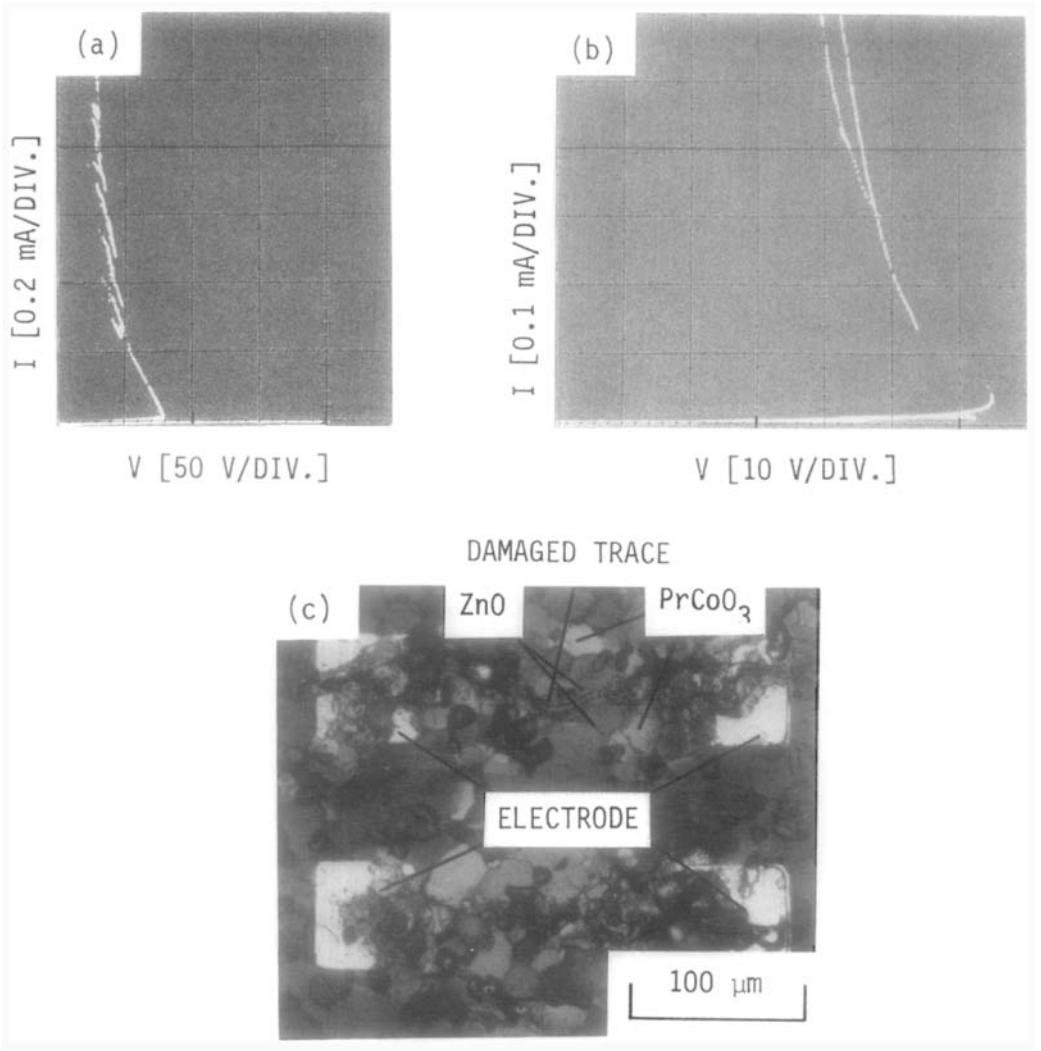

FIG. 6. Direct current-voltage traces for a combination of Co-doped ZnO and Zn-doped $PrCoO_3$ grains (a) for the first sweep and (b) after several consecutive sweeps. (c) Microstructure of combinations of Co-doped ZnO and Zn-doped $PrCoO_3$ grains after testing.

the on state were apparently low enough to avoid extensive damage to the specimen.

Figure 8 shows the relationship between dc ohmic resistivity and Co concentration for Co-doped ZnO single-phase materials prepared with the two different cobalt oxide powders. Undoped ZnO had a resistivity of around 1 Ω-cm when it was sintered in air at 1300°C. As Co content increased, the measured ohmic resistivity increased. It is important to realize that there are three possible contributions to the measured resistance of bulk polycrystalline material: (1) a possible blocking contact between the bulk and an electrode, (2) possible grain boundary region effects, and (3) the grains themselves. A series of experiments was performed to attempt to clarify which of these

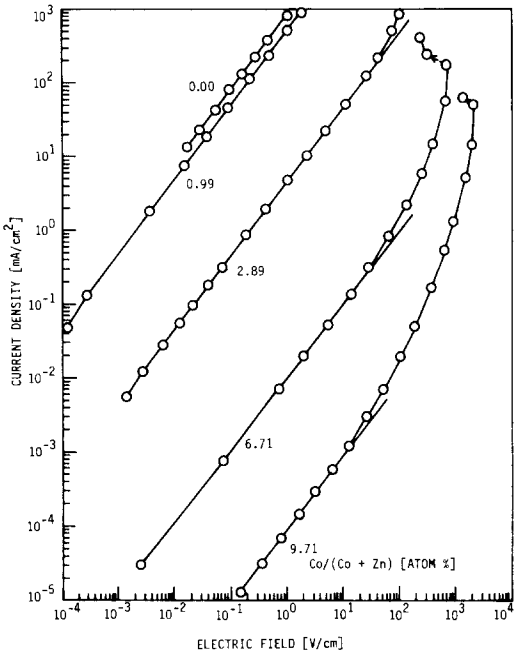

FIG. 7. Direct current-voltage characteristics of single-phase polycrystalline undoped and Co-doped ZnO (In–Ga electrodes).

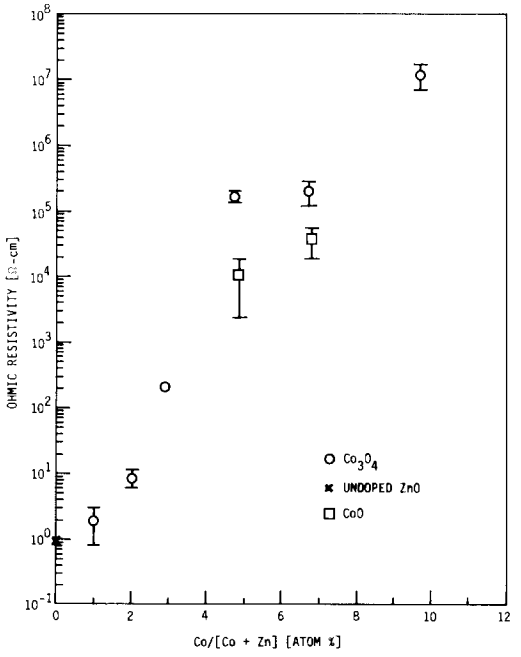

FIG. 8. Relationship between dc ohmic resistivity and Co concentration in ZnO.

sources of resistance might be contributing to the overall ohmic resistance measured for these single-phase materials. These will be described in the following paragraphs, starting with experiments designed to detect the presence of blocking electrode contacts.

One possible indication of a contribution to measured resistance from blocking contacts would be the observation of an increase in apparent resistivity with decreasing specimen thickness. Such an increase would arise because thinning the specimen would not result in a proportional reduction in overall resistance because of the relatively constant resistance due to the blocking electrodes. Figure 9 shows measured values for dc ohmic resistivity and specimen thickness for Co-doped ZnO materials fabricated with Co_3O_4 powder. The Co concentrations are indicated on the figure. The resistivity values are scattered at small

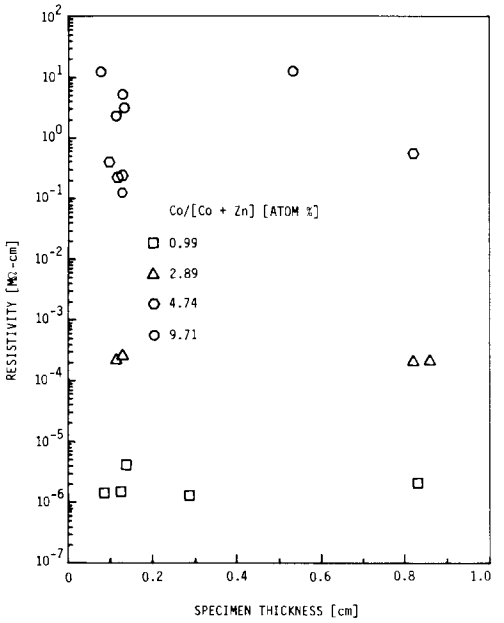

FIG. 9. Relationship between dc ohmic resistivity and specimen thickness in Co-doped ZnO.

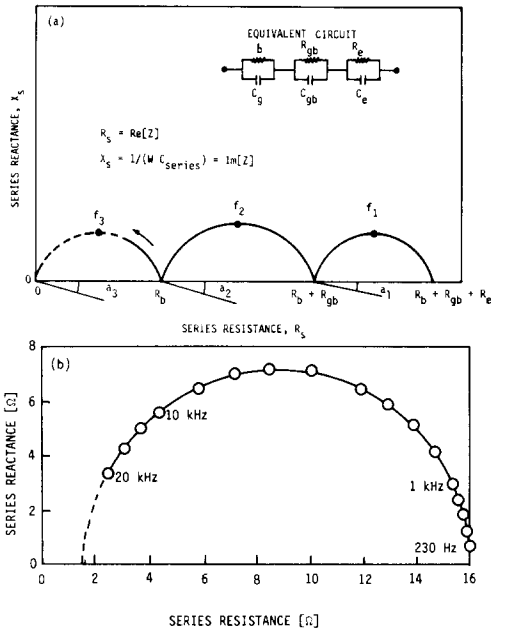

FIG. 10. (a) Idealized complex impedance diagram and corresponding equivalent circuit model (inset), and (b) typical ac complex impedance spectrum for Co-doped ZnO.

specimen thicknesses, but, at a given Co concentration, the values are essentially constant and independent of the specimen thickness for the overall range of specimen thickness. This constant resistivity is an indication that, while blocking electrode effects might make a minor contribution to measured resistance, the observed high ohmic resistivity of Co-doped ZnO material was probably a true material effect.

Ac complex impedance spectroscopy is another method which is useful to separate the sources of measured resistance of polycrystalline specimens. Figure 10a shows an ideal complex impedance spectrum and equivalent circuit. R_b is the resistance from the grains; C_g is the geometric capacitance; and R_{gb}, C_{gb}, R_e, and C_e are the lumped resistances and capacitances associated with the grain boundaries (gb) and electrodes (e), respectively. The three semicircular arcs represent dispersions at low, medium, and high frequencies caused by electrode interfacial polarization, grain boundary polarization, and grain polarization, respectively. Frequency, f, increases in the direction indicated. The center of each dispersion arc is depressed by an angle, a, which is taken as being related to the distribution of relaxation times associated with each polarization. Figure 10b shows a typical ac complex impedance spectrum of Co-doped ZnO material. Within the frequency range of the instrumentation available for this study, a single arc was observed for each specimen. The size of the arc increased as Co content increased, indicating that Co doping increased the particular impedance source in the material responsible for this arc. It is not known a priori whether the "complete" (infinite frequency range) impedance spectrum of these specimens consists of one, two, or three arcs. This depends on whether there are measurable grain boundary and/or electrode contributions to the specimen impedance. However, it is possible to make educated guesses as to how many arcs the spectrum contains, and which are actually being observed in the frequency range of this study. Extrapolation of the single observed arc to its right-hand intersection with the horizontal axis gives a resistance value corresponding closely to the measured dc bulk resistivity (which should include all resistance sources). This close agreement suggests that the single arc observed in the ac spectrum is, in fact, the lowest frequency arc in the spectrum (i.e., there most probably are no additional arcs to the right of the observed arc). It is expected that the left-hand intersection of the highest frequency arc in the total spectrum (corresponding to infinite frequency) will occur at zero resistance (Fig. 10a). Presumably, this highest frequency arc should be attributable to the impedance of the grains themselves. The observed single arc is most probably not the highest-frequency arc in

the total spectrum, because its left-hand intersection does not occur at zero resistance (see Fig. 10b). Therefore, there is indirect evidence that there is probably one or possibly two small arcs at higher frequencies (to the left) of the single observed arc. If there are actually three arcs in the total spectrum, then the observed single (lowest-frequency) arc should be attributed to electrode impedance (i.e., there is an electrode blocking contribution to dc specimen resistance). If there are only two arcs in the total spectrum, then the single observed (lowest-frequency) arc is due to grain boundary impedance, and there are no measurable electrode effects in the dc measurements. One way to discriminate between these two possibilities would be to compare the lowest frequency arcs of spectra determined with two different electrode metals of differing work function, one with greater blocking tendency than the other. If no significant differences in these lowest frequency arcs are observed with these two different electrode metals, then there probably are no electrode effects, meaning that there are only two arcs in the total spectrum, and the observed arc is due to impedance associated with the grain boundaries. On the other hand, if the lowest-frequency arc is enlarged with the more blocking type of metal electrode, the lowest-frequency arc is associated with electrode impedance, i.e., blocking contact effects are present in dc measurements. In–Ga electrodes were used to test the dc and ac characteristics of Co-doped ZnO. Since ZnO is a n-type semiconductor (as was demonstrated by hot probe measurement), a metal with a higher work function than In–Ga would have a greater blocking tendency in contact with ZnO. Gold is such a higher work-function metal. Impedance spectra measured with Au electrodes also give a single arc in the accessible frequency range, with the extrapolated low frequency end agreeing well with bulk dc resistivity (as measured also with Au electrodes), indicating that the observed arc is the lowest frequency arc. The extrapolated left-hand intersection of this arc gives resistance values about the same as was observed with In–Ga electrodes. Thus, no significant differences in lowest frequency arcs are observed with two different electrode materials, and this is a further indication that no measurable blocking contact effects were present with either electrode metal.

A possible source of impedance in a polycrystalline specimen is high resistivity material in the region around the grain boundaries. For example, there is general agreement (*13, 14*) that depletion layers formed near the boundary of ZnO grains in ZnO varistors are major barriers to conduction. In the present work, as explained above, extrapolation to the left ends of the large arcs in the impedance spectra of Co-doped ZnO materials did not lead to a zero impedance, which indicates that the observed arcs do not represent the impedance contributed by the grains themselves. Since it was also shown above that the observed arc does not appear to be associated with electrode effects, it seems most likely that the observed arc is due to the impedance of conduction barriers associated with or near the grain boundaries. If the observed arc represented the impedance from grain boundary depletion layers, it would be expected that the size of the arc would decrease as average grain size increased, because the relative fraction of material adjacent to grain boundaries decreases as grain size increases. To test this possibility, the average grain size of a Co-doped ZnO material was varied by annealing at 1300°C for up to 200 hr. Table I lists average grain size, Co concentration, and resistivity of the annealed materials measured with In–Ga electrodes. The data were very scattered, and no correlation could be determined between resistivity and average grain size. Upon annealing a specimen, total Co concentration and distribution within the grain

TABLE I

AVERAGE GRAIN SIZE, Co CONCENTRATION, AND RESISTIVITY OF Co-DOPED ZnO MATERIALS ANNEALED FOR VARIOUS TIMES

Time (hr)	AGS[a] (μm)	Co concn.[b] (atom %)	Extrapolated ac resistivity		dc ohmic resistivity (Ω-cm)
			To the left (Ω-cm)	To the right (Ω-cm)	
10	20.89	3.10	8.56	142	139
20	28.29	3.08	107.10	4.5×10^3	4.5×10^3
50	34.96	3.25	146.44	10.4×10^3	9.6×10^3
104	39.18	3.40	—[c]	181	176
204	40.36	4.50	20.85	1.3×10^3	1.2×10^3

[a] Average grain size.
[b] Co/[Co + Zn].
[c] Negative value.

changes, in addition to a reduction of the relative fraction of material adjacent to grain boundaries. Both changes will affect the total measured resistivity of bulk ZnO materials. More work is needed to understand these effects. Co concentration was observed to increase as the material was annealed for longer times, which probably indicates that the vapor pressure of ZnO is higher than that of CoO at 1300°C. No correlation was observed between resistivity and Co concentration in these annealed specimens. Values of dc resistivity were also measured on the same specimens with Au electrodes replacing In–Ga electrodes to check whether data scattering might be due to blocking contacts. The data were similar for both electrode materials.

Undoped and Zn-doped $PrCoO_3$ materials. Figure 11 shows the dc characteristics of single-phase polycrystalline undoped $PrCoO_3$ materials using three different types of electrodes: painted In-Ga, vacuum evaporated Al, and sputtered Au. The three specimens showed different characteristics even though they were all cut from the same tablet. All specimens showed ohmic behavior in the low voltage region, but the apparent ohmic resistivities for the three were quite different, as is indicated in Fig. 11. At higher voltages the specimens with In–Ga and Al electrodes showed nonohmic behavior with a slope of about 3, while the specimen with Au electrodes showed an abbreviated region of nonohmic behavior at even higher voltage. All specimens exhibited switching at similar current density values. After the specimens switched, their resistance dropped sufficiently so that very high current densities resulted, causing the specimens to break into several pieces. Even though the specimens were broken after the initial switching, reproducible switching was subsequently observed for the pieces of the original specimens. The current-voltage characteristics of the on state of the specimens could not be determined because of instrument limitations. The dc characteristics of Zn-doped $PrCoO_3$ materials were similar to those for undoped $PrCoO_3$ materials.

The differences in apparent resistivities

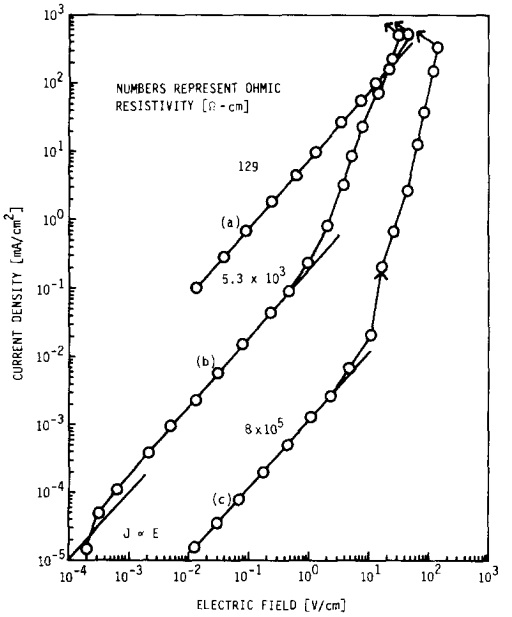

FIG. 11. Direct current-voltage characteristics of undoped single-phase polycrystalline $PrCoO_3$ determined with different electrodes: (a) Au, (b) In–Ga, (c) Al.

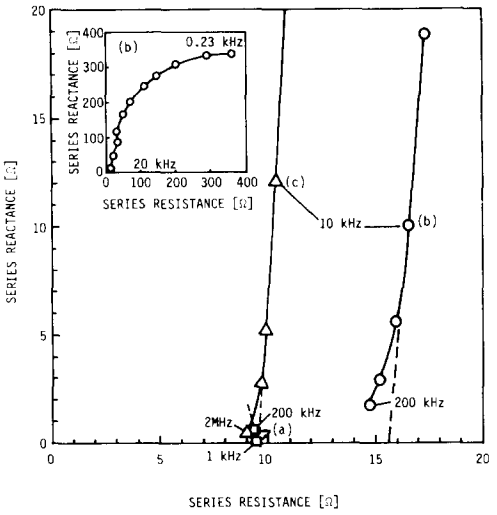

FIG. 12. Alternating current complex impedance spectra of undoped $PrCoO_3$ determined with different electrodes: (a) Au, (b) In–Ga (inset shows whole range of spectrum), and (c) Al.

of specimens of the same material measured with different electrode materials is a likely indication that blocking contacts between the specimen and the electrode contribute to the resistances of at least some of the specimens. Several techniques were used to specifically test for the presence of blocking contacts. These techniques also allowed determination of the bulk resistivity of $PrCoO_3$ materials.

Figure 12 shows a magnified plot of ac complex impedance spectra obtained for the above three samples in the 20 Ω impedance range (high frequency range). The specimens with In–Ga and Al electrodes showed a portion of a single large arc in the frequency range 230 Hz to 2 MHz. The left ends of the arcs for the specimens with In–Ga or Al electrodes did not approach zero impedance, indicating that there is at least one additional higher frequency arc in the total spectra of these specimens. Figure 12 also includes the impedance spectrum observed for the specimen with Au electrodes. The impedance data acquired for this specimen over a wide frequency range, 1 to 200 kHz, delineated only a small portion of an arc. The resistivity derived by extrapolating the arc for the Au electrode specimen to its right end was similar to the values derived by extrapolating the arcs of the In–Ga and Al electrode specimens to their left ends; therefore, both values represent bulk resistivity of the material.

As explained above, the true value of bulk resistivity of any material should be independent of the specimen thickness. Any deviation from this rule is a possible indication that electrode effects may be influencing the measurements. To test whether a blocking contact between the bulk and the electrode contributes to the observed high resistivity of specimens with In–Ga electrodes, and to determine the true value of the bulk resistivity of single-phase polycrystalline undoped $PrCoO_3$, the apparent bulk resistivities measured using different methods were related to specimen thickness. Figure 13

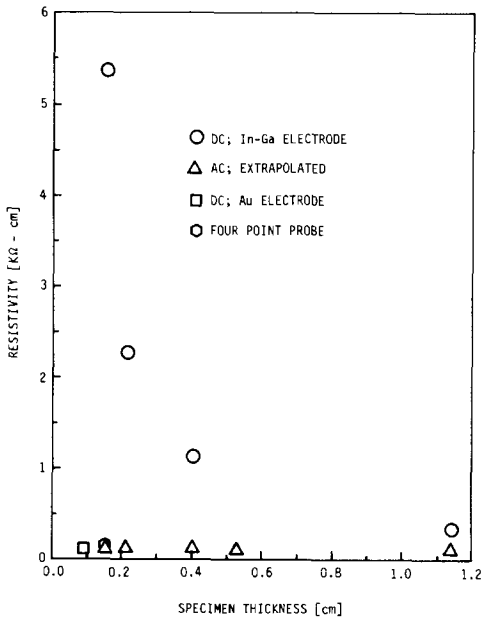

FIG. 13. Relationship between resistivity and specimen thickness for undoped $PrCoO_3$.

summarizes the resistivity-thickness observation. As thickness increased, the apparent dc resistivity of the specimens with In–Ga electrodes decreased, which is a good indication that the measured value of resistance used to calculate resistivity includes a contribution due to a blocking contact between the bulk and one of the In–Ga electrodes. The values for resistivity derived by extrapolating to the left end of the ac impedance arcs are independent of specimen thickness, indicating that this end of the arc represents either grain or a combination of grain boundary and grain resistivity. The figure also includes single resistivity values calculated from resistances measured using a four-point probe and a dc measurement made with Au electrodes. These latter resistivity values were both similar to those derived from extrapolated ac resistance and therefore are free of any blocking contact effects; these values thus give the true bulk resistivity of the material. The true value of about 100 Ω-cm is about ten times higher than a reported room temperature value for $PrCoO_3$ (*15*). This study and Ref. (*15*) used different specimen preparation conditions and resistivity measurement techniques.

To test the effect of Zn doping on the electrical characteristics of $PrCoO_3$, measurements were made on sintered Zn-doped $PrCoO_3$ oxide materials fabricated from the residue powders remaining after Co-doped ZnO grains were leached out of pulverized two-phase materials. The dc characteristics of specimens with three different electrode metals were similar to those for undoped $PrCoO_3$ (see Fig. 13), showing blocking contact effects with In–Ga and Al. Figure 14 shows a typical ac complex impedance spectrum of a Zn-doped $PrCoO_3$ specimen. Au electrodes were used in order to provide ohmic contacts. Two arcs were observed for all materials regardless of Zn content. The arcs were extrapolated using a regression procedure to determine whether the left ends of the arcs approached zero impedance. All materials showed nonzero impedance at the left ends of the observed arcs, probably indicating the presence of an additional small arc at frequencies above those available with the instruments used in this study. Thus, it was assumed that the two arcs observed were the two lowest frequency arcs in the idealized spectrum Fig. 10(a). Table II shows the extrapolated resistances assuming the ideal circuit model (inset). The table also includes data on porosity measured using a water immersion technique. Brailsford and Hohnke (*16*) analyzed the contribution to ac impedance spectra of intergranular porosity and

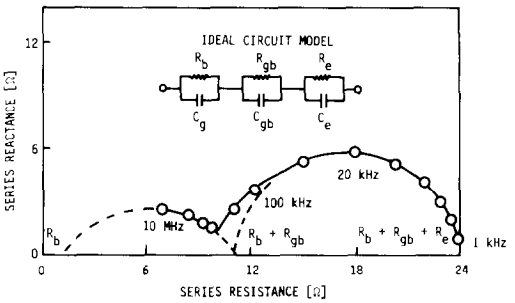

FIG. 14. Typical ac complex impedance spectrum of Zn-doped $PrCoO_3$.

TABLE II

EXTRAPOLATED RESISTANCE DATA FOR Pr–Co–Zn OXIDE MATERIALS

Weight % of ZnO in starting powder mixture[a]	R_T[b] (Ω)	R_e[c] (Ω)	$R_b + R_{gb}$ (Ω)	R_{gb}[c] (Ω)	R_b[c] (Ω)	Porosity[d] (%)
50	23.5	12.74	10.76	9.53	1.23	7.66
45	108	14.69	93.31	90.72	2.59	14.52
40	244	—[e]	244	238.55	5.45	20.73
35	76.6	7.97	68.63	62.64	5.99	12.50

[a] Amount of ZnO in starting powder mixture relates to amount of Zn in the Zn-doped $PrCoO_3$.

[b] $R_T = R_b + R_{gb} + R_e$.

[c] R_b, R_{gb}, and R_e are the resistances from the grains (b), the grain boundaries (gb), and the electrodes (e), respectively.

[d] Theoretical density of $PrCoO_3$ taken as 7.575 g/cm^3 [83].

[e] Only one arc was observed for this material.

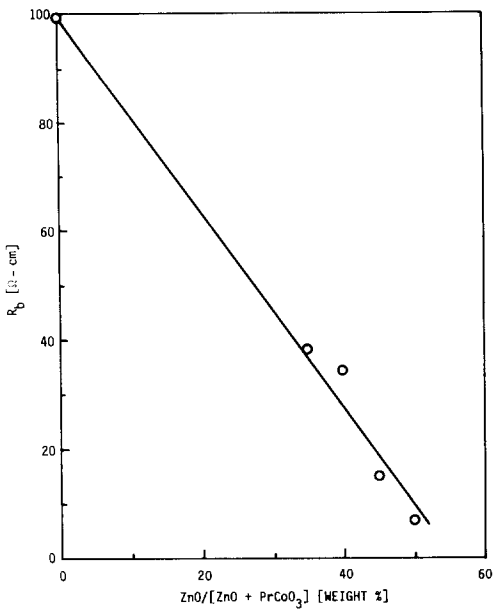

FIG. 15. Relationship between "grain" resistivity and ZnO concentration in the starting powder for Zn-doped $PrCoO_3$.

claimed that the major effect of the infinite impedance of porosity is to enlarge R_{gb}, which is normally interpreted as the resistance due to grain boundaries. Table II shows that the resistance apparently due to grain boundary polarizations, R_{gb}, increased as the total porosity for the materials increased.

Figure 15 shows the relationship between the resistivity derived from the extrapolated resistance for grains, R_b, and weight percentage of ZnO in the starting powder mixture. The resistivity was found to decrease as the content of ZnO in the original powder increased. If it is assumed that increased amounts of ZnO in the reacted powders before leaching correspond to higher levels of Zn dissolved in the $PrCoO_3$ material remaining after leaching, then Fig. 15 indicates that the grain resistivity of $PrCoO_3$ decreases as Zn content increases. This is consistent with a previous report (*17*) that Zn behaves as an acceptor in $PrCoO_3$ because of the valence difference between the dopant Zn^{2+} and the host Co^{3+}, and thereby enhances its inherent p-type conductivity.

Microstructure Model for Threshold Switching in the Two-Phase Material

When a powder mixture of $PrCoO_3$ and ZnO is sintered, Co ions from the $PrCoO_3$ diffuse into surrounding ZnO grains, and Zn ions from the ZnO diffuse into neighboring $PrCoO_3$ grains; consequently, the sintered two-phase threshold switching material consists of Co-doped ZnO and Zn-doped $PrCoO_3$ phases. Using quantitative microstructural analysis techniques (*18*), it was determined that the volume fraction of the Zn-doped $PrCoO_3$ phase in the two-phase material studied was around 25%. This value indicates that Zn-doped $PrCoO_3$ grains or clusters of them are fairly isolated from one another by surrounding Co-doped ZnO grains. Based on this observed microstructure, and on studies of the electrical characteristics of individual grains and interphase boundaries in the two-phase material, as well as the electrical characteristics of each of the single-phase polycrystalline materials which have composition similar to the individual phases of the two-phase material, a general understanding of switching in the two-phase material is possible.

Figure 16 compares the dc current-voltage characteristics of the two-phase material, a single-phase polycrystalline Co-doped ZnO material (around 10 atom% Co), and a single-phase polycrystalline Zn-doped $PrCoO_3$ material. The particular Co-doped ZnO material was chosen because it is similar in composition to Co-doped ZnO grains in the two-phase material. The particular Zn-doped $PrCoO_3$ material was arbitrarily chosen, since the electrical characteristics of $PrCoO_3$ material did not differ greatly with doping concentration compared to those of the two-phase material and Co-doped ZnO material. On the other hand, the electrical characteristics of $PrCoO_3$ did

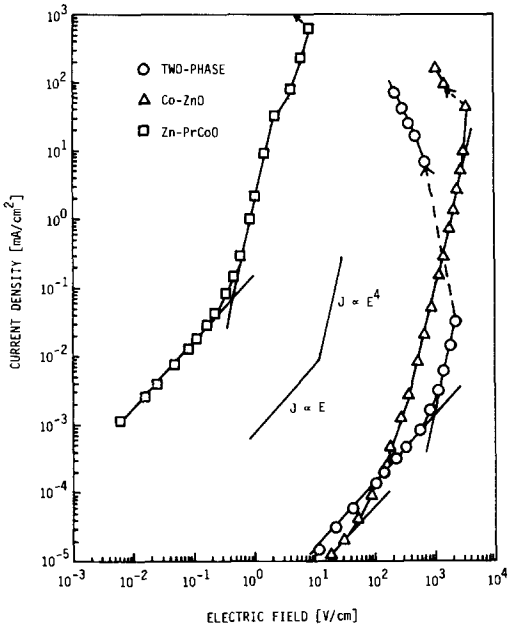

FIG. 16. Comparison of dc current-voltage characteristics of a two-phase threshold switching material, single phase Co-doped ZnO, and Zn-doped $PrCoO_3$.

change with different electrode metals. Therefore, the electrical characteristics shown in Figure 16 were all determined using the same electrode metal, In–Ga, although there is evidence of blocking tendencies with this electrode in the data of the two-phase material and the Zn-doped $PrCoO_3$ material. The three materials showed ohmic behavior at low electric fields. At higher electric fields, all three materials changed to nonohmic characteristics with nonlinear coefficients around 4, and each exhibited switching to a low-resistance on state at even higher fields. In the off state, the ohmic resistivity of the two-phase material was similar to that of the single-phase Co-doped ZnO material, but was much higher than that of the single-phase Zn-doped $PrCoO_3$ material. Because Zn-doped $PrCoO_3$ grains are more or less isolated by surrounding Co-doped ZnO grains in the two-phase material, the low resistance Zn-doped $PrCoO_3$ grains do not contribute significantly to the ohmic resistivity of the two-phase material. Instead, the high observed ohmic resistivity of the two-phase material is mainly due to the high resistance Co-doped ZnO grains.

Since the Zn-doped $PrCoO_3$ is much more conductive than the Co-doped ZnO, Zn-doped $PrCoO_3$ grains will shunt current from surrounding Co-doped ZnO grains with little voltage drop. This has the effect of concentrating the voltage drop across and current flow through Co-doped ZnO grains in the direction of the applied field. The locally intensified field and current density can initiate the filamentary conduction through the Co-doped ZnO grains, thus causing the switching. Thus the role of Zn-doped $PrCoO_3$ grains is to initiate the switching by concentrating the field and current.

Studies of the electrical characteristics of individual Co-doped ZnO grains using microelectrodes showed damage traces in the outer Co-doped region of the grains after switching. This observation suggests that the observed on state of the two-phase material is probably due to filamentary conduction in the ZnO phase, as has often been observed in other switching materials (*19*). The filament or damage trace did not follow a straight line path between the electrodes, but usually branched into two or three paths. Therefore, the effective area of the current path through the specimen in the on state is indeterminant.

The two-phase material shows a permanent reduction in threshold voltage, V_{TH}, after the first sweep, and individual Co-doped ZnO grains were shown to be conductive after being damaged by excess current in the on state. Even though the single-phase polycrystalline Co-doped ZnO specimens reported here did not show microscopic evidence of permanent breakdown damage after the initial switching, these specimens nevertheless showed a permanent reduction in threshold voltage for subsequent sweeps.

If a portion of the Co-doped ZnO phase is permanently altered during the initial sweep by high current in the on state, this would have the effect of reducing the effective thickness of the reamining high resistance material in the off state, and would be expected to result in a reduction in the threshold voltage necessary for bulk switching during subsequent sweeps. This hypothesis was supported by the further observation that the magnitude of the permanent reduction in threshold voltage of two-phase threshold switching material depended on the magnitude of the on state current permitted after the specimen switched.

Summary

A threshold switching ceramic which consisted of two major phases was identified: Co-doped ZnO and Zn-doped $PrCoO_3$. Bulk specimens of this ceramic showed high threshold switching voltage on the initial sweep and lowered but reproducible threshold voltage for subsequent sweeps. The roles of individual phases in the switching behavior of the bulk material were studied. Pristine Co-doped ZnO grains showed high resistance; however, electrical breakdown occurred at a relatively high voltage during the initial sweep, and the switched grain became permanently conductive for subsequent sweeps. Damage traces were observed after the initial switching. Zn-doped $PrCoO_3$ grains exhibited stable and reproducible threshold switching at a relatively low threshold voltage.

Undoped ZnO showed n-type semiconducting behavior with a resistivity around 1 Ω-cm. When doped with Co, the resistivity of ZnO increased, and the material exhibited threshold switching behavior. The high observed resistivity was shown not to be due to a blocking contact between the bulk material and the measuring electrodes.

Undoped and Zn-doped $PrCoO_3$ showed p-type semiconducting behavior. Blocking contact effects were observed between the bulk material and electrode metals having low work function. Reproducible threshold switching behavior was observed for undoped and Zn-doped $PrCoO_3$ materials at relatively high current density levels. The resistivity of undoped $PrCoO_3$ was around 100 Ω-cm, and decreased as Zn was added. This observation suggests that Zn in $PrCoO_3$ behaves as an acceptor due to the valence difference between the dopant and the host Co ion.

Zn-doped $PrCoO_3$ grains appear to make little contribution to the overall observed off state bulk electrical resistivity. Instead, the Co-doped ZnO grains dominate the off state electrical characteristics. However, the role of Zn-doped $PrCoO_3$ grains is to initiate the switching by concentrating the field across and current flow through Co-doped ZnO grains. The permanent reduction in threshold voltage of two-phase threshold switching material for subsequent sweeps was probably due to permanent damage in some of the Co-doped ZnO grains during the high current on state of the preceding sweep.

Acknowledgments

The authors express their sincere appreciation to Drs. Orville Hunter, Jr., Arthur V. Pohm, Mufit Akinc, and David M. Martin for useful discussions; to Ames Laboratory and Tektronix, Inc. for providing electrical measurement instruments.

References

1. M. Matsuura and T. Masuyama, *Japan J. Appl. Phys.* **14,** 889 (1975).
2. C. A. Hogarth and S. F. Anvari, *Thin Solid Films* **29,** L5 (1975).
3. T. Hada, W. Wasa, and S. Hayakawa, *Japan J. Appl. Phys.* **10,** 52 (1971).
4. O. Hunter, Jr. and J. A. Schaefer, US Patent 4472296, 1984.
5. L. Erying, *in* "Handbook on the Physics and Chemistry of Rare Earths," (K. A. Gschneidner and L. Erying, Eds.), Vol. 3, p. 337, North-Holland Publishing Company, Amsterdam, Netherlands (1979).
6. K. Eda, M. Inada, and M. Masuoka, *J. Appl. Phys.* **54,** 1095 (1983).

7. "Annual Book of ASTM Standards," Vol. 10.02, ASTM F43-83, ASTM, Philadelphia (1984).
8. "Annual Book of ASTM Standards," Vol. 10.02, ASTM F42-77, ASTM, Philadelphia (1984).
9. J. R. MACDONALD, "Superionic Conductors" (G. D. Mahan and W. L. Roth, Eds.), p. 81, Plenum Press, New York (1976).
10. "Powder Diffraction File," JCPDS, Swarthmore, PA (1980).
11. F. A. KROGER, "The Chemistry of Imperfect Crystals," 2nd ed., Vol. 2, p. 744, Elsevier/North-Holland, New York (1974).
12. H. B. MICHAELSON, *IBM J. Res. Dev.* **22,** 72 (1978).
13. "Grain Boundary Phenomena in Electronic Ceramics," (L. M. Levinson, Ed.), p. 290, The American Ceramic Society, Inc., Columbus, OH (1981).
14. M. F. YAN AND A. H. HEUER (Eds.), "Additives and Interfaces in Electronic Ceramics," p. 1, The American Ceramic Society, Inc., Columbus, OH (1983).
15. H. S. SPACIL AND C. S. TEDMON, JR., *J. Electrochem. Soc.* **116,** 1618 (1969).
16. A. P. BRAILSFORD AND D. K. HOHNKE, *Solid State Ionics* **11,** 133 (1983).
17. G. H. JONKER, *Phil. Pes. Rep.* **24,** 1 (1969).
18. W. D. KINGERY, H. K. BOWEN, AND D. R. UHLMANN, "Introduction to Ceramics," 2nd ed., p. 61, Wiley, New York, 1976.
19. A. M. BARNETT AND A. G. MILNES, *IEEE Trans. Electron Devices* **12,** 341 (1968).